

pubs.acs.org/JACS Article

Synthesis and Thin Films of Thermally Robust Quartet (S = 3/2) Ground State Triradical

Chan Shu, Maren Pink, Tobias Junghoefer, Elke Nadler, Suchada Rajca, Maria Benedetta Casu,* and Andrzej Rajca*



Cite This: J. Am. Chem. Soc. 2021, 143, 5508-5518



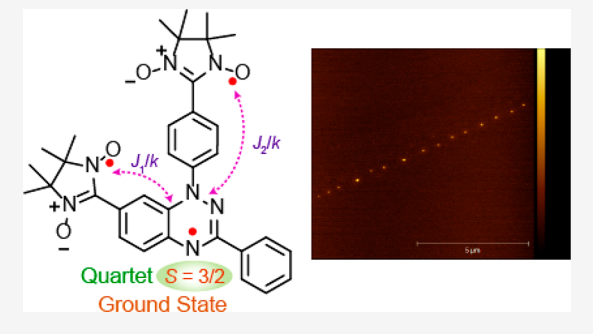
ACCESS

III Metrics & More

Article Recommendations

s Supporting Information

ABSTRACT: High-spin (S=3/2) organic triradicals may offer enhanced properties with respect to several emerging technologies, but those synthesized to date typically exhibit small doublet quartet energy gaps and/or possess limited thermal stability and processability. We report a quartet ground state triradical 3, synthesized by a Pd(0)-catalyzed radical–radical cross-coupling reaction, which possesses two doublet–quartet energy gaps, $\Delta E_{\rm DQ} \approx 0.2-0.3$ kcal mol⁻¹ and $\Delta E_{\rm DQ} 2 \approx 1.2-1.8$ kcal mol⁻¹. The triradical has a 70+% population of the quartet ground state at room temperature and good thermal stability with onset of decomposition at >160 °C under an inert atmosphere. Magnetic properties of 3 are characterized by SQUID magnetometry in polystyrene glass and by quantitative EPR spectroscopy. Triradical 3 is evaporated under ultrahigh



vacuum to form thin films of intact triradicals on silicon substrate, as confirmed by high-resolution X-ray photoelectron spectroscopy. AFM and SEM images of the ~1 nm thick films indicate that the triradical molecules form islands on the substrate. The films are stable under ultrahigh vacuum for at least 17 h but show onset of decomposition after 4 h at ambient conditions. The drop-cast films are less prone to degradation in air and have a longer lifetime.

■ INTRODUCTION

Organic radicals with high-spin ground states and large energy gap between the high-spin ground state and low-spin excited state are promising building blocks for organic magnets, ^{1–10} spintronics, ¹¹ spin filters, ^{12–14} sensors, ¹⁵ memory devices, ^{16–19} and exploration of quantum interference on molecular conductance. ²⁰ Their potential use in organic electronics depends not only on intrinsic electronic properties and stability but also on processability. Albeit the design principles for high-spin radicals are clearly established ^{21,22} and a few triplet ground state diradicals with robust stability are prepared, ^{23–27} there are only a few reports of isolated high-spin triradicals that process both good thermal stability and an energy gap between the high-spin ground state and low-spin excited state on the order of the thermal energy (*RT*) at room temperature. ^{15,28–30}

Recently, we reported the robust triplet ground state diradicals 1 and 2 (Figure 1). 31,32 To our knowledge, these and the analogous oxoverdazyl-based diradicals 33 are the only neutral high-spin diradicals that are well characterized by thermogravimetric analysis (TGA) to establish firmly their robust thermal stability. Diradicals 1 and 2 have an onset of decomposition at 175 and 160 °C, while the onset at 192 °C was reported for the oxoverdazyl-based diradical. 31–33 Diradical 2, which has a 95+% thermal population of the triplet state at room temperature, can be evaporated under ultrahigh vacuum (UHV) to form thin films on silicon. 32

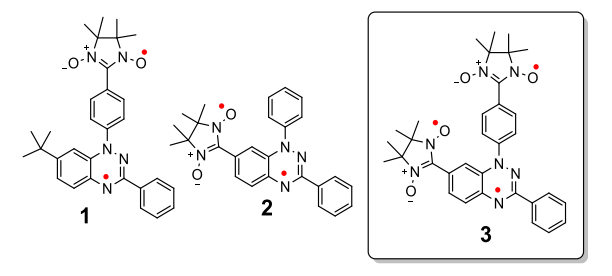


Figure 1. Thermally robust triplet ground state diradicals 1 and 2 and quartet ground state triradical 3.

The next challenge is a high-spin triradical, with a significant population of the quartet ground state at room temperature, that is suitable for thin film fabrications. The design of triradicals involves another hurdle when an additional radical extends the molecular size. The triradical must possess not only excellent thermal stability but also a molecular mass that is still under the achievable limit of evaporation temperature.³⁵

Received: February 2, 2021 Published: March 31, 2021





From our experience, ^{32,35} the controlled evaporation of diradicals is already very demanding. It would be unprecedented to successfully fabricate the first thin film of a high-spin triradical. ^{35–38}

Koutentis and co-workers recently reported the condensation-based synthesis of a Blatter-type triradical. The triradical is based on sequential connectivity of trimethylenemethane (TMM), m-phenylene, and TMM; thus, it is expected to possess nearly degenerate quartet and doublet states; that is, three S=1/2 radicals are magnetically independent. Their experimental finding of 300% spin concentration, corresponding to three S=1/2 spins, means that the triradical is composed of three S=1/2 spins that are magnetically independent at the temperature of measurement, in this case room temperature. Therefore, there is no experimental evidence for the claimed quartet ground state. The spins of the spin of the states of the spin o

The first pivotal step is the development of efficient synthetic methodologies for high-spin triradicals. Cross-couplings reactions are highly versatile and efficient methodologies in organic synthesis, relying on a metal catalyst to form a bond between two different starting materials that usually are enriched with an activating group. The development of the cross-coupling reactions in the synthesis of organic radicals has faced tremendous obstacles, largely due to the inherent reactivity of organic radicals which profoundly affect both the activation of the starting materials and the search for a suitable catalyst. Okada and co-workers recently demonstrated the Pd(0)-catalyzed cross-coupling between the gold(I)—nitronyl nitroxide complex, such as 4 (Scheme 1),

Scheme 1. Synthesis of Triradical 3 and Diradicals 2 and 8

with diamagnetic iodo-substituted aromatic compounds. 41,42 Tretyakov and co-workers also utilized complex 4 for the Pd(0)-catalyzed cross-coupling with iodo-oxoverdazyls, which led to oxoverdazyl-nitronyl nitroxide diradicals in high yields. 33 These results provide valuable insight and motivation to further develop the cross-coupling methodology for a variety of stable organic radicals. We focus on the cross-coupling reactions between Blatter radicals and nitronyl nitroxide radicals (Scheme 1).

The Blatter moiety is considerably more electron-rich compared to typical diamagnetic π -systems or oxoverdazyl

radicals (*vide infra*, Electrochemistry section). Thus, the common Pd(0) catalyst, such as Pd(PPh₃)₄ that was used by both Okada and Tretyakov, ^{33,41,42} may not be sufficiently powerful. In addition, spin delocalization in the Blatter radicals could be an impediment. The degree of spin density delocalization correlates with the strength of exchange coupling. The oxoverdazyl-nitronyl nitroxide diradicals have the smaller singlet—triplet energy gaps, $\Delta E_{\rm ST} < 0.3$ kcal mol⁻¹, ³³ compared to $\Delta E_{\rm ST} \approx 0.5$ kcal mol⁻¹ for 1 and $\Delta E_{\rm ST} \approx 1.7$ kcal mol⁻¹ for 2. ^{31,32} Thus, the spin density in the Blatter radicals is more delocalized than that in oxoverdazyls, leading to greater densities at the carbons of the C–I bonds in the starting Blatter radicals such as 5 and 6 (Scheme 1).

Here we report the synthesis and study of high-spin (S = 3/ 2) triradical 3 (Figure 1), in which we exploit the Pd(0)catalyzed radical-radical cross-coupling reactions between diiodo-substituted Blatter radical and nitronyl nitroxides. Triradical 3 has two doublet-quartet energy gaps, $\Delta E_{\rm DO} \approx$ 0.2-0.3 kcal mol⁻¹ and $\Delta E_{\rm DQ}$ $\approx 1.2-1.8$ kcal mol⁻¹, i.e., same order of magnitude as the thermal energy at room temperature, thus possessing a quartet ground state that is 70+% populated at room temperature. Triradical 3 is thermally robust, with an onset of decomposition at ~160 °C under an inert atmosphere and is thermally evaporated under ultrahigh vacuum to form thin films on SiO₂/Si(111) wafers, with X-ray photoelectron spectroscopy indicating the presence of intact 3. The AFM and SEM images of the evaporated films indicate the triradical molecules form isolated islands on the substrate, including preferential growth along a line defect of the substrate. We present here the preparation and characterization of the first thin film of high-spin (S = 3/2) organic triradical.

■ RESULTS AND DISCUSSION

Synthesis of 3. Syntheses of diradicals 1 and 2 start from the corresponding cyano-benzotriazinyl (cyano-Blatter) radicals, which are reduced to formyl-Blatter radicals and then condensed with 2,3-bis(hydroxyamino)-2,3-dimethylbutane.^{31,32,43,44} Oxidation of the condensation products yields diradicals 1 and 2, with isolated yields of 4–12% and 18–29%, respectively, for the multistep syntheses.^{31,32} An analogous approach to triradical 3, starting from the corresponding dicyano-Blatter radical, produces only miniscule quantities of triradical with ~1% yield.

The cross-coupling of di-iodo-Blatter radical, such as 5, $^{40,45-48}$ with 2+ equiv of 4 using the commonly used Pd(PPh₃)₄, with up to 60 mol % loading, $^{33,40-42}$ produces a low yield (6-17%) of triradical 3 while the coupling with 1+ equiv of 4 provides the monoiodo-substituted diradical 8 in $\sim 10\%$ isolated yield (Supporting Information). Notably, the highly reactive Pd(0)-catalyst, Pd[$(t-Bu)_3P$]₂, 49 at a 30 mol % loading in the cross-coupling reaction of 4 with 5 allows for synthesis of triradical 3 in one step in good isolated yields (Scheme 1). This approach enables a routine preparation of 3 in 100+ mg batches (Supporting Information).

We explore the cross-coupling reaction of 4 with monoiodo-Blatter radical 6^{40,45-48} using the reactive catalyst, Pd[(t-Bu)₃P]₂, which gives diradical 2 in 30-44% isolated yields (Scheme 1). We try the reactive Pd(II) catalyst, such as [1,3-bis(2,6-diisopropylphenyl)imidazol-2-ylidene](3-chloropyridyl)palladium(II) dichloride, commonly abbreviated as Pd-PEPPSI-i-Pr, in the reaction of 4 with 6, but the reaction mixtures fail to yield any detectable diradical 2.

We also examine the recently developed Pd(0)-catalyzed cross-coupling between diamagnetic iodo-substituted aromatics and nitronyl nitroxide 7 in the presence of a strong base (t-BuONa). Starting from 6, this methodology provides diradical 2 in a low yield (\sim 10%). The cross-coupling of the diiodo-Blatter radical 5 with 7 produces only monoiodo-substituted diradical 8 in low yield (\sim 1-10%), while triradical 3 is not detectable under various conditions (Supporting Information).

X-ray Crystallography. The structure of triradical 3 is supported by single-crystal X-ray analysis. Two pseudopolymorphs are analyzed, triclinic (centrosymmetric P-1) and orthorhombic ($Pna2_1$), obtained by slow evaporation of solutions of 3 in toluene/heptane and chloroform/pentane, respectively. The orthorhombic structure is a solvent polymorph, containing one molecule of chloroform. The two pseudo-polymorphs have significantly different crystal packing with the triclinic structure containing C_i -symmetric dimers of triradical molecules, while in the orthorhombic crystal structure, one-dimensional π -stacks of triradical molecules are formed (see the Supporting Information). $^{32-34,52}$

In molecules of triradical 3, both nitronyl nitroxide radical moieties are nearly coplanar with the 1,2,4-benzotriazinyl (Blatter) radical π -system (Figure 2); in both pseudopolymorphs, absolute values of N-C20-C5-C and N-C27-C11-C torsional angles are 19.8°-22.5° and 28.6°-34.1°, respectively. However, torsional angles between 1,4-phenylene rings (C8-C13) and the Blatter moiety are considerably greater, i.e., C9-C8-N1-C7 = 40.9°-49.7° and C13-C8-N1-N2 = 49.3°-51.4° (Figures S2 and S5). Consequently, the exchange coupling pathway from Blatter moiety to nitronyl nitroxide O1-N4-C20-N5-O2 (NNO1) is shorter and more coplanar than that to O3-N6-C27-N7-O4 (NNO2). Therefore, the exchange couplings associated with these two paths, J_1/k and J_2/k , are expected to be significantly different (Figure 2).

EPR Spectroscopy. The EPR spectra of 3 in glassy matrices show a quartet (S = 3/2) state, with a small admixture of thermally populated doublet (S = 1/2) state at T = 110 K (Figure 3). Because of relatively small value of zero-field splitting parameter, $D \approx 80$ MHz (Table 1), only a weak halffield $(|\Delta m_S| = 2)$ transition can be observed, and no $|\Delta m_S| = 3$ signal can be detected. 53-55 Spectral simulations confirm the purity of the triradical, ⁵⁶ that is, the absence of S = 1 or S = 1/2impurities. The spectral width for S = 3/2 triradical 3 in toluene/chloroform glass is $4D \approx 320$ MHz, which is intermediate between $2D \approx 140$ MHz for S = 1 diradical 1 and $2D \approx 480$ MHz for 2. This reflects the intermediate strength of magnetic dipole-dipole interactions in 3 that dominate the EPR spectra in glassy matrices. Similar to diradical 2, the B3LYP/EPR-II calculations of 3 not only provide an overestimated value of D = 160 MHz but also indicate the positive sign of D, which is inconsistent with the experimental EPR spectrum (Supporting Information). 32,57-62

We carry out variable temperature quantitative EPR spectroscopy on 3 in toluene/chloroform, $3:1.^{31,63}$ At each temperature in the T=110-331 K range, three independent measurements of the sample and the spin counting reference (Tempone in toluene/chloroform, 3:1) are obtained. The resultant average values of χT (mean \pm SE, n=3) are fit to the nonsymmetrical triradical model (Figure 2 and eq S1)^{30,64} using two variable parameters, exchange coupling constants, J_1/k and J_2/k , and one fixed parameter, weight correction

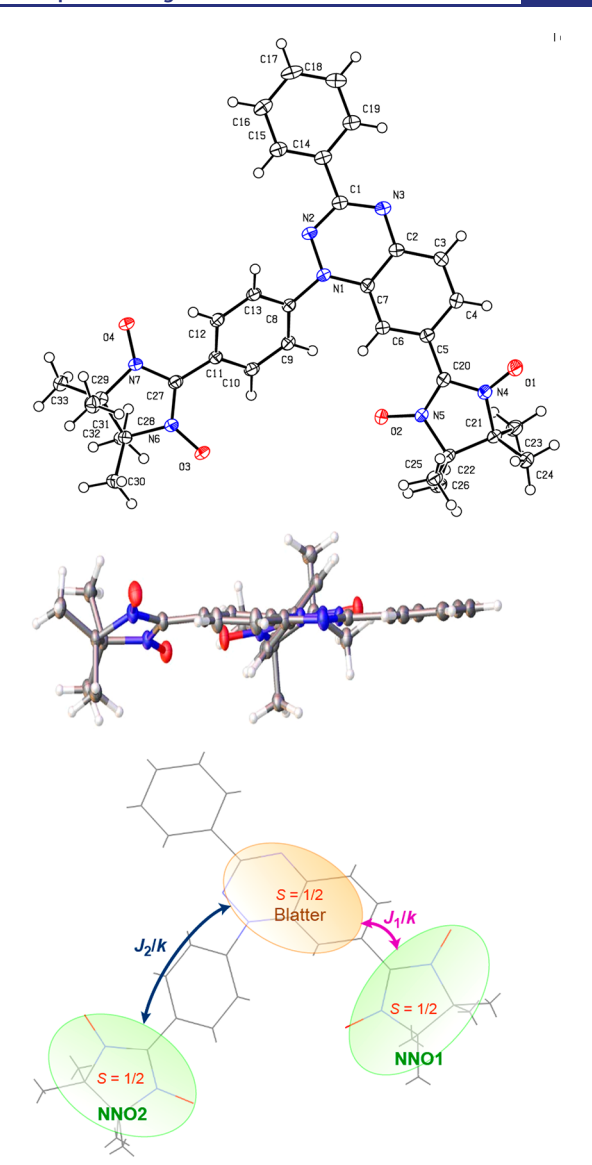


Figure 2. Single-crystal X-ray structure of triradical **3** (triclinic, centrosymmetric *P*-1 polymorph). (top) Top view, Ortep plot with carbon, nitrogen, and oxygen atoms depicted using thermal ellipsoids set at the 50% probability level. (middle) Side view of **3**. (bottom) Exchange coupling in **3**. Additional details may be found in the Supporting Information.

factor, N=0.99 (Figure 3). The parameter N accounts for an inaccurate concentration of 3 due to the uncertainty in weighing about 1 mg of the triradical sample. The value of N is derived from the spectral simulations (fits) of EPR spectra at 110 K. These fits provide the relative content of S=3/2 ground state and S=1/2 excited state, which enables an estimation of the value of χT . The ratio of the measured $\chi T=1.632\pm0.0058$ emu K mol $^{-1}$ (n=3) to the estimated $\chi T=1.6479\pm0.0003$ emu K mol $^{-1}$ (n=3) provides the value of N=0.99 (Figures S18 and S19).

Values of $J_1/k = 280 \pm 17$ K and $J_2/k = 79 \pm 2.7$ K (mean \pm SE) (Figure 4), obtained from a numerical fit to the nonsymmetrical trimer model (Figure 2 and eq S1), allow for the calculation of doublet—quartet energy gaps, $\Delta E_{\rm DQ} \approx 0.2$ kcal mol⁻¹, for the lowest S = 1/2 excited state and $\Delta E_{\rm DQ} \approx 1.2$ kcal mol⁻¹, the second lowest S = 1/2 excited state, by using eqs 1 and 2,³⁰ respectively (Table 1).

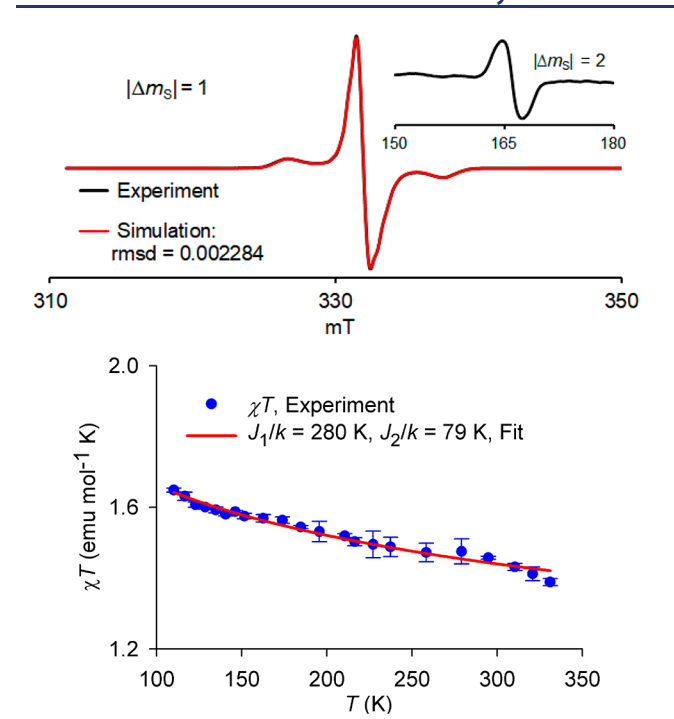


Figure 3. EPR spectroscopy of triradical 3. (top) EPR ($\nu=9.3245$ GHz) spectrum of 2.32 mM triradical 3 in 2-MeTHF glass at 105 K. The $|\Delta m_{\rm S}|=2$ transition is shown as an inset. Simulation of the $|\Delta m_{\rm S}|=1$ region: S=3/2, weight = 1.0000, D=77.84 MHz, E=22.70 MHz, $g_{xx}=2.0075$, $g_{yy}=2.0047$, $g_{zz}=2.0065$; H-strain (MHz): $H_x=15.2$, $H_y=79.3$, $H_z=47.2$; S=1/2, weight = 0.17245, $g_{xx}=2.0018$, $g_{yy}=2.0137$, $g_{zz}=1.9968$; H-strain (MHz): $H_x=10.2$, $H_y=7.1$, $H_z=17.8$. (bottom) Quantitative EPR spectroscopy of 1.36 mM 3 in toluene/chloroform (3:1). Experimental values of χT (mean \pm SE, n=3) in the T=110-331 K range and numerical two-parameter fit with two variable parameters, $J_1/k=280\pm17$ K and $J_2/k=79\pm2.7$ K (mean \pm SE). Further details are reported in eq S1 and Figures S12–S18.

$$\Delta E_{\rm DQ} = J_1 + J_2 - \left[J_1^2 + J_2^2 - (J_1 J_2)\right]^{1/2} \tag{1}$$

$$\Delta E_{\rm DQ} 2 = J_1 + J_2 + [J_1^2 + J_2^2 - (J_1 J_2)]^{1/2}$$
 (2)

SQUID Magnetometry. The quartet ground state of **3** is confirmed by SQUID studies. The χT vs T and $M/M_{\rm sat}$ vs $H/(T-\theta)$ plots for a 19 mM sample of **3** in polystyrene are shown in Figure 4.

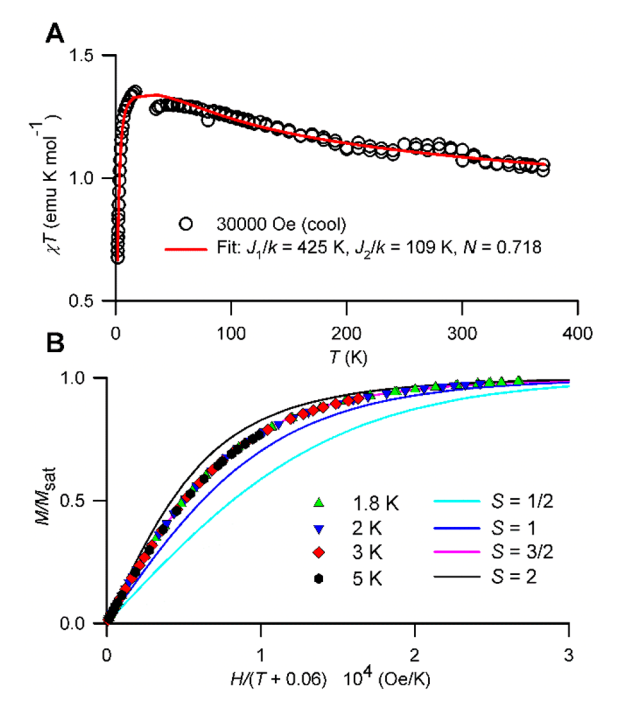


Figure 4. SQUID magnetometry of 19 mM triradical 3 in polystyrene matrix. (A) χT vs T data at H=30000 Oe in the cooling mode were fit to a triradical model (eq S1) using three variable parameters: $N=0.718\pm0.002$, $J_1/k=425\pm37$ K, and $J_2/k=109\pm4$ K (mean \pm SE), where N corresponds to weight correction factor. Downward turn in the χT vs T plot at low T is predominantly due to paramagnetic saturation. The gap in the data around 25 K corresponds to the passage through M=0 for the entire sample. (B) $M/M_{\rm sat}$ vs $H/(T-\theta)$ plot, where $\theta=-0.06$ K, at T=1.8-5 K (symbols) and the Brillouin curves corresponding to S=1/2 to 2 (lines). Further details are reported in Figures S20 and S21.

Using the nonsymmetrical triradical model, which includes the effects of paramagnetic saturation (Figure 2 and eq S1), the fits to the χT vs T data in the T=1.8-370 K range give the following values of variable parameters: $N=0.718\pm0.002$, $J_1/k=425\pm37$ K, and $J_2/k=109\pm4$ K (mean \pm SE), where N corresponds to weight correction factor (Figure 4A). The values of both J_1/k and J_2/k are greater than those obtained by EPR spectroscopy in toluene/chloroform. Consequently, larger $\Delta E_{\rm DQ} \approx 0.30$ and $\Delta E_{\rm DQ} 2 \approx 1.83$ kcal mol $^{-1}$ are obtained by using eqs 1 and 2 (Table 1). Also, these fits indicate that the

Table 1. Magnetic Characterization of Triradical 3 vs Diradicals 1 and 2

		matrix	D (MHz)	E (MHz)	J_1/k (K)	J_2/k (K)	$\Delta E_{\mathrm{DQ}}^{}a}/\Delta E_{\mathrm{ST}}$ (kcal mol ⁻¹)
3	EPR	Tol/Chl ^b	80	23	280	79	+0.22 ^a
	EPR	2-MeTHF	78	23			
	EPR	polystyrene	77	23			
	SQUID	polystyrene			425	109	+0.30 ^a
	DFT	gas phase	160°	20°			$+1.14^{d}$
2	SQUID	crystals ³²			438		$+1.74 \pm 0.07$
	SQUID	polystyrene ³²			419		$+1.68 \pm 0.16$
	EPR	Tol/Chl ^{b,32}	242	35.1			
1	SQUID	crystals ³²				126	$+0.50 \pm 0.02$
	EPR	Tol/Chl ^{b,31}	69.6	4.2		117	+0.47

 $[^]a\Delta E_{\rm DQ}$ (kcal mol $^{-1}$) determined experimentally by using eq 1. b Toluene/chloroform, 3:1. cD and E computed at the B3LYP/EPR-II level by using ORCA. 57 d BS-DFT-computed ΔE DQ at the UB3LYP/6-31G(d,p)+ZPVE level; 65 ΔE DQ2 = 1.22 (EPR) and 1.83 (SQUID) kcal mol $^{-1}$ vs 2.59 (DFT) kcal mol $^{-1}$.

intermolecular exchange interactions between molecules of 3 are negligible; i.e., the value of mean-field parameter, θ , is near zero.

Using Brillouin functions with a small mean-field parameter, $\theta=-0.06$ K, two-parameter fits to the magnetization (M) vs magnetic field (H) data, i.e., the M vs $H/(T-\theta)$ data, at low temperatures (T=1.8-5 K) provide the total spin, S=1.5 and magnetization at saturation, $M_{\rm sat}=0.736$ $\mu_{\rm B}$ ($\mu_{\rm B}=$ Bohr magneton). These data unequivocally confirm a quartet (S=3/2) ground state for 3. In addition, the value of $M_{\rm sat}=0.74$ $\mu_{\rm B}$ is comparable to N=0.72, obtained from the fit to the χT vs T data, thus indicating that the triradical is pure. Both $M_{\rm sat}$ and N are less than 1.00 because of weighing errors of 3 in the submilligram range.

A sample of 3 in benzene is investigated, in which the fits to M vs $H/(T-\theta)$ data provide the total spin, S=1.5, and indicate an S=3/2 ground state (Figure S23). Because of the relatively large mean-field parameter, $\theta\approx-1$ K, indicating relatively strong intermolecular antiferromagnetic interactions, the four-parameter fits to the χT vs T data in the relatively narrow T=1.8-260 K range are unreliable, and thus, $\Delta E_{\rm DQ}$ could not be determined.

Electrochemistry and UV-Vis-NIR Spectroscopy. Cyclic voltammetry for diradical 2 and triradical 3 in 0.1 M tetrabutylammonium hexafluorophosphate in dichloromethane at room temperature shows the presence of reversible waves associated with the oxidation of Blatter radical moieties ($E^{+/0}$ \approx +0.4 V) and nitronyl nitroxide moieties ($E^{2+/+} \approx +1.0 \text{ V}$). A reversible wave corresponding to the reduction of either the Blatter radical or the nitronyl nitroxide moiety is also observed in the $E^{-/0} \approx -0.7$ to -0.9 V range (Table S5 and Figures S9-S11). (All redox potentials are reported versus SCE.) These values are comparable to those obtained for the parent Blatter radical (+0.10 and -0.96 V) and a derivative of nitronyl nitroxide (+0.81 and -0.75 V) in acetonitrile. 18,66 Notably, $E^{+/0}$ for the oxoverdazyl radicals is about 0.4 V more positive, 33,67 and therefore they are considerably more difficult to oxidize.

UV—vis—NIR spectra of diradical 2 and triradical 3 in dichloromethane have a similar spectral pattern, consisting of three major bands at 300, 370—380, and 510—550 nm (Figure S8). The peak intensity at 371 nm ($\varepsilon_{\rm max}=2.26\times10^4~{\rm L~mol}^{-1}~{\rm cm}^{-1}$) for 3 is about twice that at 381 nm ($\varepsilon_{\rm max}=1.3\times10^4~{\rm L~mol}^{-1}~{\rm cm}^{-1}$) for diradical 2. The intense 371 nm peak is associated with the band originating from the phenyl-substituted nitronyl nitroxide, which usually appears at 362 nm ($\varepsilon_{\rm max}=1.77\times10^4~{\rm L~mol}^{-1}~{\rm cm}^{-1}$) in hexane or at 360 nm ($\varepsilon_{\rm max}=1.33\times10^4~{\rm L~mol}^{-1}~{\rm cm}^{-1}$) in ethanol. Biradical 2 and triradical 3 have nearly identical absorption onsets in the 860—880 nm range, corresponding to an optical gap, $E_{\rm g}=1.42\pm0.01~{\rm eV}$ (mean \pm SE). The UV—vis—NIR spectrum for triradical 3 could be reproduced by the TD-DFT computation at the UCAM-B3LYP/6-31+G(d,p)/IEF-PCM-UFF level of theory employing a dichloromethane solvent model (Figure S26).

Thermal Stability. Triradical 3 possesses excellent stability at ambient conditions. It can be purified by chromatography using normal phase silica gel. Thermogravimetric analysis data suggest that thermal decomposition of 3 starts at 166 °C (1% mass loss), which is slightly higher than the onset temperature for diradical 2 (Figure 5) and lower than that for diradical 1. The maximum rate of mass loss for 3 is at 180 °C.

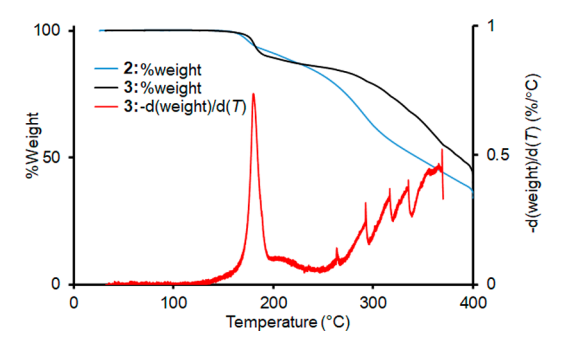


Figure 5. Thermogravimetric analysis (TGA) of triradical 3 under N_2 ; heating rate = 5 °C min⁻¹.

Thin Films of 3 on SiO₂/Si(111) Substrate. An important prerequisite of the technological applications foreseen for this class of materials requires attaching molecules to a substrate, to form either an interface or a film. A controlled and clean way to achieve this goal is by using controlled evaporation. We have previously focused our efforts on the evaporation of radicals and diradicals. ^{32,35–38,69–72}

Here, we extend our protocol to evaporate triradical 3. We deposit thin films of triradical 3 on SiO₂/Si(111) wafers by organic molecular beam deposition (OMBD).⁷³ which has been proven to be a suitable method for growing radical and diradical thin films. However, increasing the number of radical sites implies an increased reactivity during evaporation, making it extremely challenging. 35,38 We investigate the obtained thin films by X-ray photoelectron spectroscopy (XPS), an effective and powerful tool for studies of organic and organic radical thin films.³⁸ We adopt the approach that was previously used for the diradical thin films to assess the intactness of triradical 3 in the films.^{32,35} We also obtain the films by drop-casting deposition. Fabrication of films by the two growth methods allows exploring the differences due to preparation and thickness range. The C 1s and N 1s core level curves are shown in Figure 6 that also includes the fit components. In fact, XPS is sensitive to the stoichiometry of the films; identifying the contributions associated with each element in its chemical environment helps to gain information about the

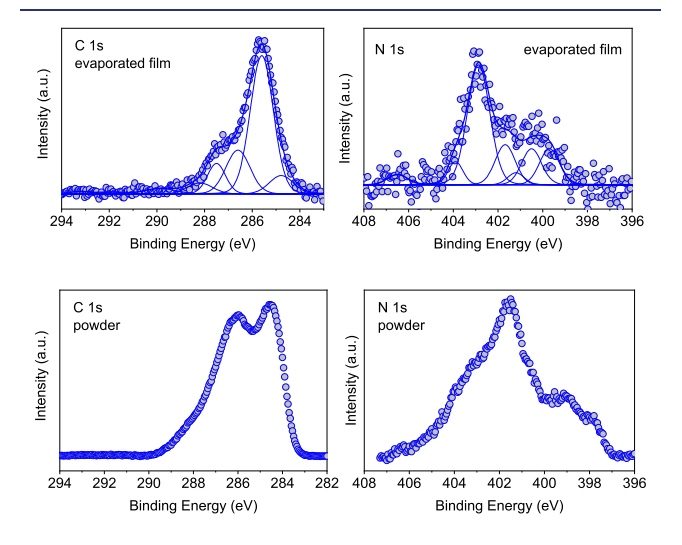


Figure 6. Typical C 1s and N 1s core level XPS spectra of triradical 3 deposited on $SiO_2/Si(111)$ wafers (0.4 nm thick film, nominal thickness) (top plots) together with the fit analysis compared to the powder spectra (bottom plots).

chemical composition of the films after evaporation (the fit procedure is described step by step in refs 32 and 74). The elemental concentration of the films calculated from the XPS spectra agrees very well with the stoichiometry of the triradical (carbon 84.4% and nitrogen 16.6% as obtained from XPS versus the stoichiometric 82.5% and 17.5%, respectively). This agreement is further supported by the fit results of the single contributions due to photoelectrons emitted by atoms with different chemical environment that shows the expected intensities in the main line (Tables S6 and S7). Note that we do not consider the O 1s spectroscopic line because it is a superposition of the signal from the films and the substrate making its fit analysis speculative.

The C 1s spectrum of the evaporated films is characterized by a main line at around 285.5 eV due to photoelectrons emitted from the atoms in the aromatic ring and the carbon atoms bound to hydrogen atoms (C–C, C–H, and CH₃). The shoulder at higher binding energy is due to contributions from the electrons emitted from carbon atoms bound also to nitrogen (C–N).

Nitrogen atoms, because of their higher electronegativity, shift the electronic cloud; thus, the electrons are emitted with lower kinetic energy, i.e., higher binding energy. The N 1s core level spectrum shows contributions due to seven nitrogen atoms: the three nitrogen atoms belonging to the Blatter radical have different chemical environments, while the two nitrogen atoms belonging to the nitronyl nitroxide (NN) radical have equivalent chemical environments. 32,35,72,75 These differences give rise to a complex spectrum with two broad features, showing the highest intensity at around 402.5 eV that corresponds to the line expected in the NN radical N 1s core level spectrum.⁷² We also observe the presence of satellites; they are typical features in photoemission that appear as an effect of the relaxation processes due to the creation of a core hole. 76,77 On the basis of the comparison of the film fit results (Tables S6 and S7) and the molecular stoichiometry, we can conclude that there is no degradation of the triradical molecules during evaporation and deposition, under the present conditions.

The comparison with the powder spectra also indicates that the evaporation and the deposition of the film are successful. We note that the XPS curves of the powder are affected by a strong charging effect. This effect is expected in organic crystals because of the absence of efficient screening of the core hole. Here this effect is very strong, leading to a broadening of the features and changes in the line intensities. We noticed similarly strong charging effects also in the XPS curves of diradical 2 that may be viewed as a fusion of the Blatter radical with a single nitronyl nitroxide radical, therefore having two radical moieties in common with triradical 3.

XPS also offers the opportunity to identify *in situ* the thin film growth mode following the decay of the substrate signal during evaporation. We follow the XPS core level signal of the substrate (Si 2p) by looking at its attenuation upon film deposition (Figure 7). The curve is characterized by a very slow decay. This intensity trend hints at a Volmer–Weber (VW) growth mode, i.e., island growth. This result is consistent with the *ex situ* atomic force microscopy (AFM) and the scanning electron microscope (SEM) images obtained for triradical 3 films (Figure 7), which are clearly showing a film morphology dominated by islands. The VW growth mode occurs when the interaction between the deposited molecules is much stronger than between the molecules and the

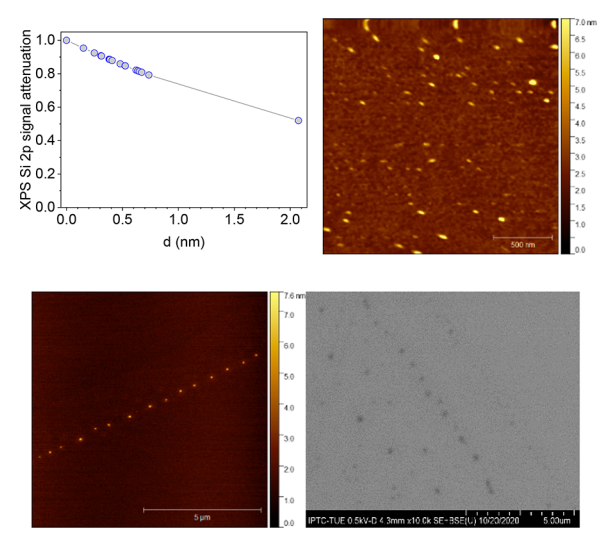


Figure 7. (upper panels) Attenuation of the Si 2p XPS signal, normalized to the corresponding saturation signal, as a function of film nominal thickness, deposition at room temperature (the line is a guide to the eye). A typical 2 μ m × 2 μ m AFM image of a film (0.4 nm nominally thick film, bottom panel). (lower panels) A 10 μ m × 10 μ m AFM image of a film (0.7 nm nominally thick film) showing the island decorating a line defect of the substrate, together with the corresponding SEM image.

substrate. We have observed this growth mode for all thin films of radicals and diradicals that we have previously investigated, grown on $SiO_2/Si(111)$ wafers, keeping the substrate at room temperature. However, the tendency to grow isolated islands increases from radicals to diradicals, ^{32,35} and now it is confirmed by the present results on triradical 3.

We also observe that the nonstoichiometric films, resulting from failed evaporations of 3, show a different island morphology. The microscopy investigations (Figure S24) suggest that different stoichiometry leads to different molecule—molecule interactions and plays a central role in the film morphology.

We investigate the drop-cast films using the same techniques. XPS spectra of the film (Figure 8) show the same features as those in the spectra of the evaporated samples. The results further affirm that the evaporation does not degrade the triradical. The fit procedure supports the expected result of films having elemental concentrations in agreement with the stoichiometry of the triradical (Tables S8 and S9). The AFM images as well as the SEM images are featureless and flat (over the examined field of view) as expected for the drop-cast preparation. The SEM images that comprise a larger area are characterized by distributed circular valleys, as typically observed in films obtained by using this processing method, due to the drying effects caused by the solvent evaporation (Figure 8).

Finally, we monitor the lifetime of the films in UHV (base pressure 2×10^{-10} mbar) by using XPS, focusing on the N 1s core level spectrum that is correlated to the nitronyl nitroxide and Blatter radicals. We adopt the protocol previously applied to radical and diradical films. 32,35,74 We observe no major changes in the spectra of the evaporated films after their exposure to UHV at room temperature for around 17 h (Figure S25). However, after 4 h of air exposure, we observe major changes in their XPS spectra, indicating film degradation (Figure S25). Thus, the triradical thin films are much less

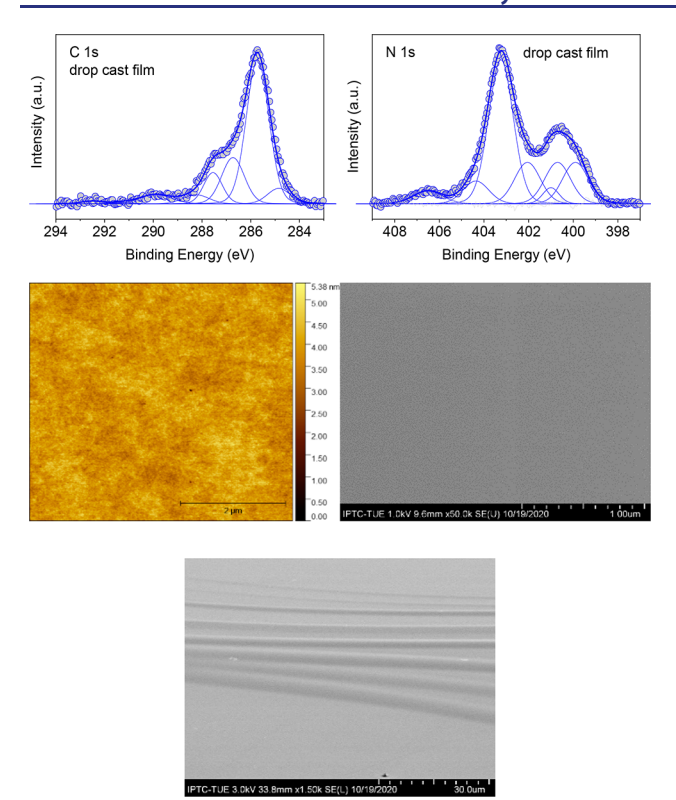


Figure 8. (upper panels) C 1s and N 1s core level XPS spectra of a drop-cast film of triradical 3 deposited on $SiO_2/Si(111)$ wafers (top plots) together with the fit analysis. (middle panels) A typical featureless 5 μ m \times 5 μ m AFM image of a drop-cast film with the corresponding SEM image. (lower panel) A typical SEM image showing the circular valleys due to the drying effects.

robust in air. We have found that diradical thin films have shorter lifetime in air than their monoradical analogues. (Nitronyl nitroxide and the Blatter monoradical derivatives showed changes in their XPS after the films were kept for several weeks/months at ambient conditions. This tendency is now also found for the evaporated triradical 3 films

The drop-cast film N 1s core level spectra change on a longer time scale when exposed to air. These changes are different, however, rather than showing different line shapes as in the case of the evaporated films; there is a change in the relative intensities of the two broad features (Figure S25), which may be due to structural changes. We also observe changes in the intensity of the satellite features that would support this hypothesis. 81,82 In addition, the changes in N 1s core level spectra tend to saturate after 84 h. Also, the adsorption of ambient nitrogen may contribute to the changes of the core level line intensities. Because the drop-cast films are thicker by 2 orders of magnitude than the evaporated films (nanometers versus hundreds of nanometers), we may speculate that the changes in intensities originate from the degradation of the more superficial layers of the drop-cast films. These degraded layers then act as a protective buffer for the underneath material that keeps its properties.

CONCLUSION

We have synthesized a high-spin triradical 3 by the radical—radical cross-coupling reaction between di-iodo-substituted Blatter radical and nitronyl nitroxide derivative. We show that

at room temperature 70+% of the triradical molecules populate the high-spin, S = 3/2, ground state. The triradical possesses a remarkable thermal stability to permit fabrication of intact triradical thin films on silicon substrate via evaporation under ultrahigh vacuum. The triradical molecules form isolated islands on the substrate with the tendency to decorate the substrate line defects, which might be useful for fabrication of nanostructured functionalized surfaces. The triradical films are stable under ultrahigh vacuum; however, within a few hours of exposure to air, XPS of the films show major changes. The drop-cast films show longer air lifetime. We have demonstrated that it is possible to evaporate triradicals and deposit their thin films under controlled conditions without degradation. The triradical films are less stable compared to the films of diradical 2 or nitronyl nitroxide and Blatter monoradicals. Our triradical, with an unprecedented combination of high-spin ground state and thermal properties, which is suitable for thin film fabrication under ultrahigh vacuum, could facilitate the development of purely organic magnetic and electronic materials.

■ EXPERIMENTAL SECTION

(Nitronyl nitroxide-2-ido) (triphenylphosphine) gold(I) (4) is synthesized by the reaction of nitronyl nitroxide (7) and $\mathrm{Au^I(PPh_3)Cl}$ with NaOH in methanol/dichloromethane. After purification by chromatography (deactivated $\mathrm{Al_2O_3}$), the spin concentration of 4 is up to 99%. Di-iodo-Blatter radical 5 and its monoiodo analogue 6 are prepared according to previous literature.

Frozen and liquid solution EPR spectra were obtained by using a Bruker EMX-plus X-band spectrometer and simulated with the EasySpin software. TGA instrument (TA Instruments TGA 550) was run either without or with IR attachment (Thermo NICOLET Is50 NIR). Variable temperature (from 1.8 up to 370 K) magnetic susceptibility measurements of 3 were performed by using a Quantum Design SQUID magnetometer with applied magnetic fields of 30000 and 5000 Oe. Variable field (0–50000 Oe) magnetization studies were performed at temperatures of 1.8–5 K. Sample tubes for SQUID studies in dilute matrices are described in the Supporting Information.

X-ray Crystallography. Crystals of 3 for X-ray studies were prepared by slow evaporation from solution in in toluene/heptane and chloroform/pentane. Data collections were performed at 100 K at either the Advanced Photon Source, Argonne National Laboratory, by using $\lambda = 0.41328$ Å synchrotron radiation (silicon monochromators) or the Indiana University by using Mo K α radiation. Following integration (SAINT), ⁸⁶ the intensity data were corrected for absorption (SADABS). The space groups for two polymorphs, P-1 and $Pna2_1$, were determined based on intensity statistics and the systematic absences. The structures were solved (SHELTX) ⁸⁸ and then refined on F2 (SHELXL). ⁸⁹ Crystal and structure refinement data for two polymorphs of 3 are in the Supporting Information and the deposited (CCDC #s: 2062663 and 2062664) files in CIF format.

Synthesis of Triradical 3. Standard techniques for synthesis under inert atmosphere (argon or nitrogen) using custom-made Schlenk glassware, custom-made double manifold high-vacuum lines, argon-filled MBraun glovebox, and nitrogen-filled glovebags. Chromatographic separations were performed by using either normal phase silica gel or neutral alumina.

Triradical **3**. A mixture of Blatter radical **5** (200.0 mg, 0.373 mmol, 1 equiv) and nitronyl nitroxide radical **4** (500.0 mg, 0.821 mmol, 2.2 equiv) was added to a Schlenk tube and evacuated on vacuum line for several minutes. The tube was kept under vacuum, and then it was transferred to the antichamber of the glovebox. Inside the argon-filled glovebox, palladium(0) catalyst $(Pd[P(t-Bu)_3]_2, 57.0 \text{ mg}, 30 \text{ mol }\%)$ was added into the tube. Freshly distilled, dry THF was added into the tube under an argon gas flow. The reaction mixture was stirred at room temperature for 48 h. The dark red solution was evaporated to

provide a dark solid, which was purified by silica gel column chromatography using dichloromethane, followed by 10% ethyl acetate in dichloromethane, as eluents. The resultant solid was washed with pentane to give 93.1 mg (42%) of product 3 as a dark solid. TLC (silica gel, ethyl acetate): R_f 0.43. HR-TOF-MS: m/z, [M + Na]+ calcd for C₃₃H₃₆N₇O₄Na 617.2726; found, 617.2728 (0.3 ppm, RA = 100%). IR (powder, cm⁻¹): 2981.51, 2937.11, 1599.50, 1518.83, 1480.79, 1448.57, 1419.16, 1392.11, 1363.07, 1310.84, 1271.29, 1254.60, 1194.33, 1130.93, 1069.11, 1025. 05, 1017.26, 952.98, 919.95, 863.37, 834.99, 823.22, 788.48, 699.98. 2981.51, 2937.11, 1599.50, 1518.83, 1480.79, 1448.57, 1419.16, 1392.11, 1363.07, 1310.84, 1271.29, 1254.60, 1194.33, 1130.93, 1069.11, 1025. 05, 1017.26, 952.98, 919.95, 863.37, 834.99, 823.22, 788.48, 699.98. The spin concentration was determined to be 378% ($\chi T = 1.42$ emu K mol-1) in toluene/chloroform (4:1) fluid solution at 294 K and 435% ($\chi T = 1.63 \text{ emu K mol}^{-1}$) at 110 K in toluene/chloroform (3:1) glass. For each measurement, TEMPONE in the identical solvent was used as a spin counting reference. Because we use S = 1/2monoradical as reference (100% spin concentration), for an S = 3/2 triradical with perfectly populated quartet ground state spin concentration should be $100\%[3/2 \times (3/2 + 1)]/[1/2 \times (1/2 + 1)]$ = 500%; in other words, the signal intensity (or χT) should correspond to five independent monoradicals. Values of <500% reflect thermal population of the excited doublet states.

Computational Details. All geometry optimizations for 3 were performed at the UB3LYP/6-31G(d,p) level of theory in the gas phase or with Gaussian 16 default IEF-PCM solvent model for toluene, tetrahydrofuran, or ethanol (Table S10). Obtained minima were confirmed by frequency calculations. The broken-symmetry approach was applied for open-shell doublet calculations, and spin contamination errors were corrected by approximate spin-projection method. 90,91 Broken symmetry doublet wave functions ($\langle S^2 \rangle \approx 1.8$) at the UB3LYP/6-31G(d,p)+ZPVE level of theory were checked for stability. All calculations were performed with the Gaussian 16 program suite. 65

Thin Film Growth, XPS, and Microscopy Measurements. Thin films were deposited on native SiO2 grown on single-side polished n-Si(111) wafers. The films were evaporated via OMBD by using a Knudsen cell under UHV conditions. The UHV apparatus used for deposition and XPS measurements is composed of dedicated preparation and measurement (base pressure $\bar{3} \times 10^{-10}$ mbar) chambers. The measurement chamber is equipped with a monochromatic Al K α source (SPECS Focus 500) and a hemispherical electron analyzer (SPECS Phoibos 150). The wafers were cleaned by sonication for an hour each in ethanol and acetone and subsequent annealing at ca. 500 K in UHV and verification of cleanness by XPS. The nominal films thicknesses of the evaporated films were calculated from the attenuation of the substrate signal. Drop-cast films of triradical 3 from 50 µL of toluene solution with a concentration of 2-3 mg/mL were deposited on the substrates with an area of about 1 cm² under ambient conditions. Their thickness (100-250 nm) was estimated with a scratch test by using SEM images. For the preparation of powder samples indium foil was used into which the powder was firmly pressed to minimize the charging of the crystals. Pass energies of 50 and 20 eV were used for survey spectra and individual core level spectra, respectively. Spectra were calibrated to the Si 2p signal at 99.8 eV and the In 3d signal at 103.3 eV depending on the used substrate. Radiation damage was minimized by only measuring freshly prepared samples and limiting beam exposure. Beam exposure in measurements aimed to investigate the stability of the films was further reduced to attribute changes solely to the degradation by air or in UHV. This leads to a worse signal-to-noise ratio. Atomic force microscopy (AFM) was measured in air with a Digital Instruments Nanoscope III Multimode AFM using tapping mode and ScanAsyst mode. Scanning electron microscopy (SEM) was measured by using a HITACHI SU8030 ultrahigh resolution field emission scanning electron microscope.

ASSOCIATED CONTENT

Supporting Information

The Supporting Information is available free of charge at https://pubs.acs.org/doi/10.1021/jacs.1c01305.

General procedures and materials, additional experimental details, fit results for the energy positions and relative intensities of the photoemission lines in the C 1s and N 1s spectra; AFM and SEM microscopy of thin films; UHV and air film lifetime (PDF)

Accession Codes

CCDC 2062663-2062664 contain the supplementary crystallographic data for this paper. These data can be obtained free of charge via www.ccdc.cam.ac.uk/data_request/cif, or by emailing data_request@ccdc.cam.ac.uk, or by contacting The Cambridge Crystallographic Data Centre, 12 Union Road, Cambridge CB2 1EZ, UK; fax: +44 1223 336033.

AUTHOR INFORMATION

Corresponding Authors

Andrzej Rajca — Department of Chemistry, University of Nebraska, Lincoln, Nebraska 68588-0304, United States; orcid.org/0000-0002-8856-1536; Email: arajca1@unl.edu

Maria Benedetta Casu — Institute of Physical and Theoretical Chemistry, University of Tübingen, 72076 Tübingen, Germany; orcid.org/0000-0002-5659-7040; Email: benedetta.casu@uni-tuebingen.de

Authors

Chan Shu – Department of Chemistry, University of Nebraska, Lincoln, Nebraska 68588-0304, United States

Maren Pink – Department of Chemistry, Indiana University, Bloomington, Indiana 47405-7102, United States

Tobias Junghoefer – Institute of Physical and Theoretical Chemistry, University of Tübingen, 72076 Tübingen, Germany

Elke Nadler – Institute of Physical and Theoretical Chemistry, University of Tübingen, 72076 Tübingen, Germany

Suchada Rajca – Department of Chemistry, University of Nebraska, Lincoln, Nebraska 68588-0304, United States;

orcid.org/0000-0003-0904-8329

Complete contact information is available at: https://pubs.acs.org/10.1021/jacs.1c01305

Notes

The authors declare no competing financial interest.

ACKNOWLEDGMENTS

We thank the National Science Foundation (NSF), Chemistry Division, for support of this research under Grants CHE-1665256 and CHE-1955349 (A.R.) and the National Institutes of Health (NIGMS #R01GM124310-01 to S.R. and A.R.) for the upgrade of EPR spectrometer. Support for the acquisition of the Bruker Venture D8 diffractometer through the Major Scientific Research Equipment Fund from the President of Indiana University and the Office of the Vice President for Research is gratefully acknowledged. NSF's ChemMatCARS Sector 15 is supported by the Divisions of Chemistry (CHE) and Materials Research (DMR), National Science Foundation, under Grant NSF/CHE-1834750. Use of the Advanced Photon Source, an Office of Science User Facility operated for the U.S. Department of Energy (DOE) Office of Science by

Argonne National Laboratory, was supported by the U.S. DOE under Contract DE-AC02-06CH11357. We also thank Thomas Chassé for accessing the photoelectron laboratory at the University of Tübingen. Financial support from the German Research Foundation (DFG) under Contract CA852/11-1 is gratefully acknowledged. We thank Dr. N. M. Gallagher for initial trials in the synthesis of triradical 3 by using the condensation method and Dr. Hui Zhang for sample preparations for SQUID measurements.

REFERENCES

- (1) Rajca, A.; Wongsriratanakul, J.; Rajca, S. Magnetic ordering in an organic polymer. *Science* **2001**, *294*, 1503–1505.
- (2) Ratera, L.; Veciana, J. Playing with organic radicals as building blocks for functional molecular materials. *Chem. Soc. Rev.* **2012**, *41*, 303–349.
- (3) Wingate, A. J.; Boudouris, B. W. Recent advances in the syntheses of radical-containing macromolecules. *J. Polym. Sci., Part A: Polym. Chem.* **2016**, *54*, 1875–1894.
- (4) Rajca, A. Organic diradicals and polyradicals: from spin coupling to magnetism? *Chem. Rev.* **1994**, *94*, 871–893.
- (5) Rajca, A. The Physical Organic Chemistry of Very High-Spin Polyradicals. *Adv. Phys. Org. Chem.* **2005**, 40, 153–199.
- (6) Gallagher, N. M.; Olankitwanit, A.; Rajca, A. High-Spin Organic Molecules. *J. Org. Chem.* **2015**, *80*, 1291–1298.
- (7) Rajca, A.; Lu, K.; Rajca, S. High-spin polyarylmethyl polyradical: Fragment of a macrocyclic 2-strand based upon calix[4]arene rings. *J. Am. Chem. Soc.* **1997**, *119*, 10335–10345.
- (8) Rajca, S.; Rajca, A.; Wongsriratanakul, J.; Butler, P.; Choi, S. Organic Spin Clusters. Dendritic-Macrocyclic Polyarylmethyl Polyradical with Very High-Spin of S = 10 and its Derivatives: Synthesis, Magnetic Studies, and Small Angle Neutron Scattering. *J. Am. Chem. Soc.* **2004**, *126*, 6972–6986.
- (9) Rajca, A.; Wongsriratanakul, J.; Rajca, S.; Cerny, R. L. Organic Spin Clusters: Annelated Macrocyclic Polyarylmethyl Polyradicals and Polymer with Very High-Spin S = 6-18. Chem. Eur. J. **2004**, 10, 3144–3157.
- (10) Rajca, A.; Wongsriratanakul, J.; Rajca, S. Organic Spin Clusters: Macrocyclic-Macrocyclic Polyarylmethyl Polyradicals with Very High-Spin S=5-13. *J. Am. Chem. Soc.* **2004**, *126*, 6608–6626.
- (11) Sanvito, S. Molecular spintronics. Chem. Soc. Rev. 2011, 40, 3336-3355.
- (12) Shil, S.; Bhattacharya, D.; Misra, A.; Klein, D. J. A high-spin organic diradical as a spin filter. *Phys. Chem. Chem. Phys.* **2015**, *17*, 23378–23383.
- (13) Herrmann, C.; Solomon, G. C.; Ratner, M. A. Organic Radicals as Spin Filters. J. Am. Chem. Soc. 2010, 132, 3682–3684.
- (14) Hu, G.; Xie, S.; Wang, C.; Timm, C. Spin-dependent transport and functional design in organic ferromagnetic devices. *Beilstein J. Nanotechnol.* **2017**, *8*, 1919–1931.
- (15) Gaudenzi, R.; Burzuri, E.; Reta, D.; Moreira, I. d. P. R.; Bromley, S. T.; Rovira, C.; Veciana, J.; van der Zant, H. S. J. Exchange Coupling Inversion in a High-Spin Organic Triradical Molecule. *Nano Lett.* **2016**, *16*, 2066–2071.
- (16) Yonekuta, Y.; Susuki, K.; Oyaizu, K.; Honda, K. Battery-Inspired, Nonvolatile, and Rewritable Memory Architecture: a Radical Polymer-Based Organic Device. *J. Am. Chem. Soc.* **2007**, *129*, 14128–14129.
- (17) Oyaizu, K.; Nishide, H. Radical Polymers for Organic Electronic Devices: A Radical Departure from Conjugated Polymers? *Adv. Mater.* **2009**, *21*, 2339–2344.
- (18) Lee, J.; Lee, E.; Kim, S.; Bang, G. S.; Shultz, D. A.; Schmidt, R. D.; Forbes, M. D. E.; Lee, H. Nitronyl Nitroxide Radicals as Organic Memory Elements with Both n- and p-Type Properties. *Angew. Chem., Int. Ed.* **2011**, *50*, 4414–4418.
- (19) Gaudenzi, R.; de Bruijckere, J.; Reta, D.; Moreira, I. d. P. R.; Rovira, C.; Veciana, J.; van der Zant, H. S. J.; Burzuri, E. Redox-

- Induced Gating of the Exchange Interactions in a Single Organic Diradical. ACS Nano 2017, 11, 5879–5883.
- (20) Tsuji, Y.; Hoffmann, R.; Strange, M.; Solomon, G. C. Close relation between quantum interference in molecular conductance and diradical existence. *Proc. Natl. Acad. Sci. U. S. A.* **2016**, *113*, E413–F419
- (21) Borden, W. T.; Davidson, E. R. Effects of electron repulsion in conjugated hydrocarbon diradicals. *J. Am. Chem. Soc.* **1977**, *99*, 4587–4594.
- (22) Ovchinnikov, A. A. Multiplicity of the ground state of large alternant organic molecules with conjugated bonds (do organic ferromagnets exist?). *Theor. Chim. Acta* **1978**, 47, 297–304.
- (23) Inoue, K.; Iwamura, H. 2-[p-(N-tert-butyl-N-oxyamino)-phenyl]-4,4,5,5-tetramethyl-4,5-dihydroimidazol-3-oxide-l-oxyl, a stable diradical with a triplet ground state. *Angew. Chem., Int. Ed. Engl.* 1995, 34, 927–928.
- (24) Shultz, D. A.; Fico, R. M.; Lee, H.; Kampf, J. W.; Kirschbaum, K.; Pinkerton, A. A.; Boyle, P. D. Mechanisms of exchange modulation in trimethylenemethane-type biradicals: The roles of conformation and spin density. *J. Am. Chem. Soc.* **2003**, *125*, 15426—15432.
- (25) Rajca, A.; Shiraishi, K.; Vale, M.; Han, H.; Rajca, S. Stable Hydrocarbon Diradical, an Analogue of Trimethylenemethane. *J. Am. Chem. Soc.* **2005**, *127*, 9014–9020.
- (26) Suzuki, S.; Furui, T.; Kuratsu, M.; Kozaki, M.; Shiomi, D.; Sato, K.; Takui, T.; Okada, K. Nitroxide-substituted nitronyl nitroxide and iminonitroxide. *J. Am. Chem. Soc.* **2010**, *132*, 15908–15910.
- (27) Kato, K.; Furukawa, K.; Osuka, A. A Stable Trimethylenemethane Triplet Diradical Based on a Trimeric Porphyrin Fused π -System. *Angew. Chem., Int. Ed.* **2018**, *57*, 9491–9494.
- (28) Shimizu, D.; Osuka, A. A Benzene-1,3,5-Triaminyl Radical Fused with Zn-II-Porphyrins: Remarkable Stability and a High-Spin Quartet Ground State. *Angew. Chem., Int. Ed.* **2018**, *57*, 3733–3736.
- (29) Ishida, T.; Iwamura, H. Bis[3-tert-butyl-5-(*N*-oxy-tert-butylamino)phenyl] nitroxide in a quartet ground state: a prototype for persistent high-spin poly[(oxyimino)-1,3-phenylenes]. *J. Am. Chem. Soc.* **1991**, *113*, 4238–4241.
- (30) Tanaka, M.; Matsuda, K.; Itoh, T.; Iwamura, H. Syntheses and Magnetic Properties of Stable Organic Triradicals with Quartet Ground States Consisting of Different Nitroxide Radicals. *J. Am. Chem. Soc.* **1998**, 120 (29), 7168–7173.
- (31) Gallagher, N. M.; Bauer, J. J.; Pink, M.; Rajca, S.; Rajca, A. High-spin organic diradical with robust stability. *J. Am. Chem. Soc.* **2016**, *138*, 9377–9380.
- (32) Gallagher, N.; Zhang, H.; Junghoefer, T.; Giangrisostomi, E.; Ovsyannikov, R.; Pink, M.; Rajca, S.; Casu, M. B.; Rajca, A. Thermally and Magnetically Robust Triplet Ground State Diradical. *J. Am. Chem. Soc.* 2019, 141, 4764–4774.
- (33) Tretyakov, E. V.; Zhivetyeva, S. I.; Petunin, P. V.; Gorbunov, D. E.; Gritsan, N. P.; Bagryanskaya, I. Y.; Bogomyakov, A. S.; Postnikov, P. S.; Kazantsev, M. S.; Trusova, M. E.; Shundrina, I. K.; Zaytseva, E. V.; Parkhomenko, D. A.; Bagryanskaya, E. G.; Ovcharenko, V. I. Ferromagnetically Coupled S = 1 Chains in Crystals of Verdazyl-Nitronyl Nitroxide Diradicals. *Angew. Chem., Int. Ed.* **2020**, *59*, 20704–20710.
- (34) Wang, W.; Chen, C.; Shu, C.; Rajca, S.; Wang, X.; Rajca, A. S = 1 Tetraazacyclophane Diradical Dication with Robust Stability: a Case of Low Temperature One-Dimensional Antiferromagnetic Chain. *J. Am. Chem. Soc.* **2018**, *140*, 7820–7826.
- (35) Junghoefer, T.; Gallagher, N.; Kolanji, K.; Giangrisostomi, E.; Ovsyannikov, R.; Chassé, T.; Baumgarten, M.; Rajca, A.; Calzolari, A.; Casu, M. B. Challenges in controlled thermal deposition of organic diradicals. *Chem. Mater.* **2021**, 33, 2019.
- (36) Huang, Z.; Zhang, Y.; He, Y.; Song, H.; Yin, C.; Wu, K. A chemist's overview of surface electron spins. *Chem. Soc. Rev.* **2017**, 46 (7), 1955–1976.
- (37) Ciccullo, F.; Gallagher, N. M.; Geladari, O.; Chasse, T.; Rajca, A.; Casu, M. B. A Derivative of the Blatter Radical as a Potential

- Metal-Free Magnet for Stable Thin Films and Interfaces. ACS Appl. Mater. Interfaces 2016, 8, 1805–1812.
- (38) Casu, M. B. Nanoscale Studies of Organic Radicals: Surface, Interface, and Spinterface. *Acc. Chem. Res.* **2018**, *51*, 753–760.
- (39) Zissimou, G. A.; Berezin, A. A.; Manoli, M.; Nicolaides, C.; Trypiniotis, T.; Koutentis, P. A. 3,3',3''-(Benzene-1,3,5-triyl)tris(1-phenyl-1H-benzo[e][1,2,4]triazin-4-yl): A C_3 symmetrical Blattertype triradical. *Tetrahedron* **2020**, 76, 131077. Our additional concerns include EPR spectra simulation, thermal stability characterization, and DFT computations. We repeated the UB3LYP computations of doublet—quartet energy gap and obtained the broken-symmetry doublet with $\langle S^2 \rangle$ of 1.80, as expected, and the energy gap of only 0.17 kcal mol⁻¹ (eq S2). Because this level of theory overestimates stability of high spin ground state (*vide infra*), this tridradical might turn out to be a low-spin (doublet) ground state, very close in energy to the excited quartet (ref 4).
- (40) Constantinides, C. P.; Koutentis, P. A.; Loizou, G. Synthesis of 7-aryl/heteraryl-1,3-diphenyl-1,2,4-benzotriazinyls via palladium catalyzed Stille and Suzuki-Miyaura reactions. *Org. Biomol. Chem.* **2011**, *9*, 3122–3125.
- (41) Tanimoto, R.; Suzuki, S.; Kozaki, M.; Okada, K. Nitronyl Nitroxide as a Coupling Partner: Pd-Mediated Cross-coupling of (Nitronyl nitroxide-2-ido)(triphenylphosphine)gold(I) with Aryl Halides. *Chem. Lett.* **2014**, *43*, 678–680.
- (42) Tahara, T.; Suzuki, S.; Kozaki, M.; Shiomi, D.; Sugisaki, K.; Sato, K.; Takui, T.; Miyake, Y.; Hosokoshi, Y.; Nojiri, H.; Okada, K. Triplet Diradical-Cation Salts Consisting of the Phenothiazine Radical Cation and a Nitronyl Nitroxide. *Chem. Eur. J.* **2019**, *25*, 7201–7209
- (43) Osiecki, J. H.; Ullman, E. F. Studies of free radicals. I. alpha. Nitronyl nitroxides, a new class of stable radicals. *J. Am. Chem. Soc.* **1968**, *90*, 1078–1079.
- (44) Rajca, A.; Pink, M.; Mukherjee, S.; Rajca, S.; Das, K. 1,3-Alternate calix[4]arene nitronyl nitroxide tetraradical and diradical: synthesis, X-ray crystallography, paramagnetic NMR spectroscopy, EPR spectroscopy, and magnetic studies. *Tetrahedron* **2007**, *63*, 10731–10742.
- (45) Bodzioch, A.; Zheng, M.; Kaszyński, P.; Utecht, G. Functional Group Transformations in Derivatives of 1,4-Dihydrobenzo[1,2,4]-triazinyl Radical. *J. Org. Chem.* **2014**, *79*, 7294–7310.
- (46) Koutentis, P. A.; Lo Re, D. Catalytic Oxidation of *N*-Phenylamidrazones to 1,3-Diphenyl-1,4-dihydro-1,2,4-benzotriazin-4-yls: An Improved Synthesis of Blatter's Radical. *Synthesis* **2010**, 2010, 2075–2079
- (47) Constantinides, C. P.; Koutentis, P. A. Stable N- and N/S-Rich Heterocyclic Radicals: Synthesis and Applications. *Adv. Heterocycl. Chem.* **2016**, *119*, 173–207.
- (48) Rogers, F. J. M.; Norcott, P. L.; Coote, M. L. Recent advances in the chemistry of benzo[e][1,2,4]triazinyl radicals. *Org. Biomol. Chem.* **2020**, *18*, 8255–8277.
- (49) Fleckenstein, C. A.; Plenio, H. Sterically demanding trialkylphosphines for palladium-catalyzed cross coupling reactions—alternatives to PtBu₃. *Chem. Soc. Rev.* **2010**, *39*, 694–711.
- (50) Suzuki, S.; Nakamura, F.; Naota, T. Environmentally Benign Strategy for Arylation of Nitronyl Nitroxide Using a Non-Transition Metal Nucleophile. *Org. Lett.* **2020**, *22* (4), 1350–1354.
- (51) Constantinides, C. P.; Lawson, D. B.; Zissimou, G. A.; Berezin, A. A.; Mailman, A.; Manoli, M.; Kourtellaris, A.; Leitus, G. M.; Clérac, R.; Tuononen, H. M.; Koutentis, P. A. Polymorphism in a π stacked Blatter radical: structures and magnetic properties of 3-(phenyl)-1-(pyrid-2-yl)-1,4-dihydrobenzo[e][1,2,4]triazin-4-yl. *CrystEngComm* **2020**, 22, 5453–5463.
- (52) Rajca, A.; Takahashi, M.; Pink, M.; Spagnol, G.; Rajca, S. Conformationally constrained, stable, triplet ground state (S=1) nitroxide diradicals: antiferromagnetic chains of S=1 diradicals. *J. Am. Chem. Soc.* **2007**, 129, 10159–10170.
- (53) Rajca, A.; Utamapanya, S. Poly(arylmethyl) Quartet Triradicals and Quintet Tetraradicals. J. Am. Chem. Soc. 1993, 115, 2396–2401.

- (54) Rajca, A.; Rajca, S.; Desai, S. R. Macrocyclic)-Conjugated Carbopolyanions and Polyradicals Based upon Calix[4]arene and Calix[3]arene Rings. *J. Am. Chem. Soc.* **1995**, *117*, 806–816.
- (55) Rajca, S.; Rajca, A. Novel High-Spin Molecules: R-Conjugated Polyradical Polyanions. Ferromagnetic Spin Coupling and Electron Localization. J. Am. Chem. Soc. 1995, 117, 9172–9179.
- (56) Stoll, S.; Schweiger, A. EasySpin, a comprehensive software package for spectral simulation and analysis in EPR. *J. Magn. Reson.* **2006**, *178*, 42–55.
- (57) Neese, F. The ORCA program system. Wiley Interdisciplinary Reviews: Comp. Mol. Sci. 2012, 2, 73–78.
- (58) Sinnecker, S.; Neese, F. Spin-Spin Contributions to the Zero-Field Splitting Tensor in Organic Triplets, Carbenes and Biradicals A Density Functional and Ab Initio Study. *J. Phys. Chem. A* **2006**, *110*, 12267–12275.
- (59) Rajca, A.; Olankitwanit, A.; Rajca, S. Triplet Ground State Derivative of Aza-m-Xylylene Diradical with Large Singlet-Triplet Energy Gap. J. Am. Chem. Soc. 2011, 133, 4750–4753.
- (60) Olankitwanit, A.; Pink, M.; Rajca, S.; Rajca, A. Synthesis of Azam-Xylylene Diradicals with Large Singlet-Triplet Energy Gap and Statistical Analyses of their EPR Spectra. *J. Am. Chem. Soc.* **2014**, *136*, 14277–14288.
- (61) Olankitwanit, A.; Rajca, S.; Rajca, A. Aza-m-Xylylene Diradical with Increased Steric Protection of the Aminyl Radicals. *J. Org. Chem.* **2015**, *80*, 5035–5044.
- (62) Rajca, A.; Olankitwanit, A.; Wang, Y.; Boratynski, P. J.; Pink, M.; Rajca, S. High-Spin S=2 Ground State Aminyl Tetraradicals. *J. Am. Chem. Soc.* **2013**, *135*, 18205–18215.
- (63) Shu, C.; Zhang, H.; Olankitwanit, A.; Rajca, S.; Rajca, A. High-Spin Diradical Dication of Chiral π -Conjugated Double Helical Molecule. *J. Am. Chem. Soc.* **2019**, *141*, 17287–17294.
- (64) Belorizky, E; Fries, P. Exact solutions for simple spin clusters with isotropic Heisenberg exchange interactions. *J. Chim. Phys. Phys.-Chim. Biol.* **1993**, *90*, 1077–1100.
- (65) Frisch, M. J.; Trucks, G. W.; Schlegel, H. B.; Scuseria, G. E.; Robb, M. A.; Cheeseman, J. R.; Scalmani, G.; Barone, V.; Petersson, G. A.; Nakatsuji, H.; Li, X.; Caricato, M.; Marenich, A. V.; Bloino, J.; Janesko, B. G.; Gomperts, R.; Mennucci, B.; Hratchian, H. P.; Ortiz, J. V.; Izmaylov, A. F.; Sonnenberg, J. L.; Williams-Young, D.; Ding, F.; Lipparini, F.; Egidi, F.; Goings, J.; Peng, B.; Petrone, A.; Henderson, T.; Ranasinghe, D.; Zakrzewski, V. G.; Gao, J.; Rega, N.; Zheng, G.; Liang, W.; Hada, M.; Ehara, M.; Toyota, K.; Fukuda, R.; Hasegawa, J.; Ishida, M.; Nakajima, T.; Honda, Y.; Kitao, O.; Nakai, H.; Vreven, T.; Throssell, K.; Montgomery, J. A., Jr.; Peralta, J. E.; Ogliaro, F.; Bearpark, M. J.; Heyd, J. J.; Brothers, E. N.; Kudin, K. N.; Staroverov, V. N.; Keith, T. A.; Kobayashi, R.; Normand, J.; Raghavachari, R.; Rendell, A. P.; Burant, J. C.; Iyengar, S. S.; Tomasi, J.; Cossi, M.; Millam, J. M.; Klene, M.; Adamo, C.; Cammi, R.; Ochterski, J. W.; Martin, R. L.; Morokuma, K.; Farkas, O.; Foresman, J. B.; Fox, D. J. Gaussian 16, Revision A.03; Gaussian, Inc.: Wallingford, CT, 2016.
- (66) Hutchison, K. A.; Srdanov, G.; Menon, R.; Gabriel, J.-C. P.; Knight, B.; Wudl, F. A Pressure Sensitive Two-Dimensional Tetracyanoquinodimethane (TCNQ) Salt of a Stable Free Radical. *J. Am. Chem. Soc.* **1996**, *118*, 13081–13082.
- (67) Gilroy, J. B.; McKinnon, S. D. J.; Koivisto, B. D.; Hicks, R. G. Electrochemical Studies of Verdazyl Radicals. *Org. Lett.* **2007**, *9*, 4837–4840.
- (68) Ullman, E. F.; Osiecki, J. H.; Boocock, D. G. B.; Darcy, R. Studies of Stable Free Radicals. X. Nitronyl Nitroxide Monoradicals and Biradicals as Possible Small Molecule Spin Labels. *J. Am. Chem. Soc.* 1972, 94, 7049–7059.
- (69) Kakavandi, R.; Calzolari, A.; Borozdina, Y. B.; Ravat, P.; Chassé, T.; Baumgarten, M.; Casu, M. B. Unraveling the mark of surface defects on a spinterface: The nitronyl nitroxide/ $TiO_2(110)$ interface. *Nano Res.* **2016**, *9*, 3515–3527.
- (70) Kakavandi, R.; Ravat, P.; Savu, S. A.; Borozdina, Y. B.; Baumgarten, M.; Casu, M. B. Electronic Structure and Stability of Fluorophore-Nitroxide Radicals from Ultrahigh Vacuum to Air Exposure. *ACS Appl. Mater. Interfaces* **2015**, *7* (3), 1685–1692.

- (71) Caneschi, A.; Casu, M. B. Substrate-induced effects in thin films of a potential magnet composed of metal-free organic radicals deposited on Si(111). *Chem. Commun.* **2014**, *50* (88), 13510–13513.
- (72) Savu, S.-A.; Biswas, I.; Sorace, L.; Mannini, M.; Rovai, D.; Caneschi, A.; Chassé, T.; Casu, M. B. Nanoscale Assembly of Paramagnetic Organic Radicals on Au(111) Single Crystals. *Chem. Eur. J.* 2013, 19 (10), 3445–3450.
- (73) Forrest, S. R. Ultrathin Organic Films Grown by Organic Molecular Beam Deposition and Related Techniques. *Chem. Rev.* **1997**, 97 (6), 1793–1896.
- (74) Junghoefer, T.; Nowik-Boltyk, E. M.; de Sousa, J. A.; Giangrisostomi, E.; Ovsyannikov, R.; Chassé, T.; Veciana, J.; Mas-Torrent, M.; Rovira, C.; Crivillers, N.; Casu, M. B. Stability of radical-functionalized gold surfaces by self-assembly and on-surface chemistry. *Chemical Science* **2020**, *11* (34), 9162–9172.
- (75) Ciccullo, F.; Calzolari, A.; Bader, K.; Neugebauer, P.; Gallagher, N. M.; Rajca, A.; van Slageren, J.; Casu, M. B. Interfacing a Potential Purely Organic Molecular Quantum Bit with a Real-Life Surface. *ACS Appl. Mater. Interfaces* **2019**, *11* (1), 1571–1578.
- (76) Enkvist, C.; Lunell, S.; Sjögren, B.; Brühwiler, P. A.; Svensson, S. The C1s shakeup spectra of Buckminsterfullerene, acenaphthylene, and naphthalene, studied by high resolution x-ray photoelectron spectroscopy and quantum mechanical calculations. *J. Chem. Phys.* 1995, 103 (15), 6333–6342.
- (77) Sjogren, B.; Svensson, S.; de Brito, A. N.; Correia, N.; Keane, M. P.; Enkvist, C.; Lunell, S. The C1s core shake-up spectra of alkene molecules: An experimental and theoretical study. *J. Chem. Phys.* **1992**, *96* (9), 6389–6398.
- (78) Barth, G.; Linder, R.; Bryson, C. Advances in charge neutralization for XPS measurements of nonconducting materials. *Surf. Interface Anal.* **1988**, *11* (6–7), 307–311.
- (79) Bauer, E. Phänomenologische Theorie der Kristallabscheidung an Oberflächen. Z. Kristallogr. 1958, 110 (1–6), 372–394.
- (80) Venables, J. A. Introduction to Surface and Thin Film Processes.; Cambridge University Press: Cambridge, 2000.
- (81) Casu, M. B.; Schuster, B.-E.; Biswas, I.; Raisch, C.; Marchetto, H.; Schmidt, T.; Chassé, T. Locally Resolved Core-hole Screening, Molecular Orientation, and Morphology in Thin Films of Diindenoperylene Deposited on Au(111) Single Crystals. *Adv. Mater.* **2010**, 22 (33), 3740–3744.
- (82) Arantes, C.; Chernick, E. T.; Gruber, M.; Rocco, M. L. M.; Chasse, T.; Tykwinski, R. R.; Casu, M. B. Interplay between solution-processing and electronic structure in metal-free organic magnets based on a TEMPO pentacene derivative. *J. Phys. Chem. C* **2016**, *120* (6), 3289–3294.
- (83) Boocock, D. G. B.; Darcy, R.; Ullman, E. F. Studies of free radicals. II. Chemical properties of nitronylnitroxides. A unique radical anion. *J. Am. Chem. Soc.* **1968**, *90*, 5945–5946.
- (84) Tretyakov, E. V.; Utepova, I. A.; Varaksin, M. V.; Tolstikov, S. E.; Romanenko, G. V.; Bogomyakov, A. S.; Stass, D. V.; Ovcharenko, V. I.; Chupakhin, O. N. New approach to synthesis of nitronyl and imino nitroxides based on S_NH methodology. *ARKIVOC* **2011**, *2011*, 76–98.
- (85) Rajca, A.; Mukherjee, S.; Pink, M.; Rajca, S. Exchange Coupling Mediated Through-Bonds and Through-Space in Conformationally-Constrained Polyradical Scaffolds: Calix[4]arene Nitroxide Tetraradicals and Diradical. J. Am. Chem. Soc. 2006, 128, 13497—13507.
- (86) SAINT v. 2018.1; Bruker AXS: Madison, WI, 2018.
- (87) SADABS v. 2018.1; Bruker AXS: Madison, WI, 2018.
- (88) Sheldrick, G. M. SHELXT Integrated space-group and crystal structure determination. *Acta Crystallogr., Sect. A: Found. Adv.* **2015**, 71, 3–8.
- (89) Sheldrick, G. M. Crystal structure refinement with SHELXL. Acta Crystallogr., Sect. C: Struct. Chem. 2015, 71, 3–8.
- (90) Trinquier, G.; Suaud, N.; Malrieu, J.-P. Theoretical Design of High-Spin Polycyclic Hydrocarbons. *Chem. Eur. J.* **2010**, *16*, 8762–8772.
- (91) Yamaguchi, K.; Jensen, F.; Dorigo, A.; Houk, K. N. A Spin Correction Procedure for Unrestricted Hartree-Fock and Møller-

Plesset Wavefunctions for Singlet Diradicals and Polyradicals. *Chem. Phys. Lett.* **1988**, *149*, 537–542.